

## Supporting Information

### **Oxygen-defect-rich coating with nanoporous texture as both anode host and artificial SEI for dendrite-mitigated lithium-metal batteries**

Qingping Wu,<sup>a,b</sup> Zhenguo Yao,<sup>b,d</sup> Aochen Du,<sup>c</sup> Han Wu,<sup>b</sup> Minsong Huang,<sup>b,d</sup> Jun Xu,<sup>a</sup> Fahai Cao,<sup>a,\*</sup> and Chilin Li<sup>b,d,\*</sup>

<sup>a</sup> State Key Laboratory of Chemical Engineering, East China University of Science and Technology, Shanghai 200237, China

E-mail: [fhcao@ecust.edu.cn](mailto:fhcao@ecust.edu.cn)

<sup>b</sup> State Key Laboratory of High Performance Ceramics and Superfine Microstructure, Shanghai Institute of Ceramics, Chinese Academy of Sciences, 585 He Shuo Road, Shanghai 201899, China

E-mail: [chilinli@mail.sic.ac.cn](mailto:chilinli@mail.sic.ac.cn)

<sup>c</sup>Key Laboratory of Transparent Opto-functional Inorganic Materials, Shanghai Institute of Ceramics, Chinese Academy of Sciences, Shanghai, China.

<sup>d</sup> Center of Materials Science and Optoelectronics Engineering, University of Chinese Academy of Sciences, Beijing 100049, China.

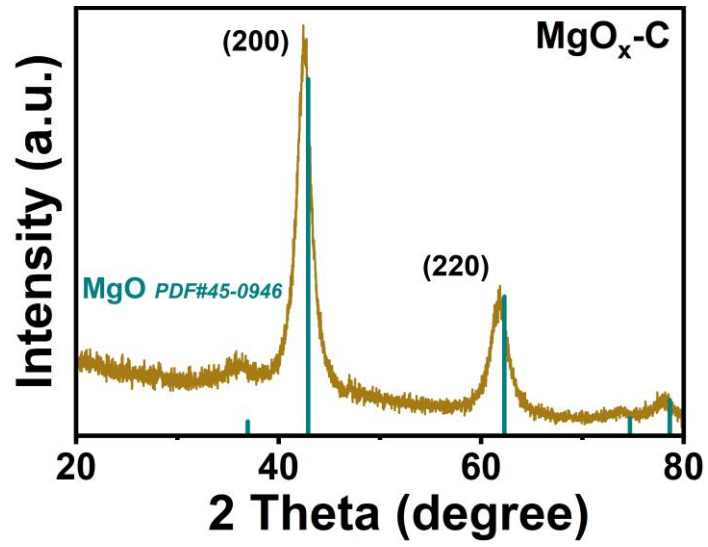


**Figure S1.** XRD pattern of MgO<sub>x</sub>-C.

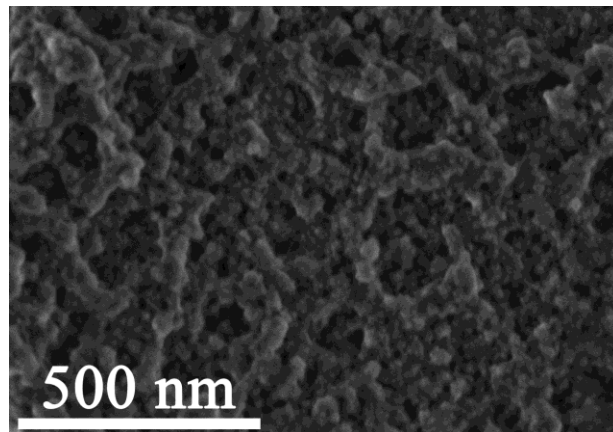


**Figure S2.** SEM image of MgO<sub>x</sub>-C with nanoporous structure.

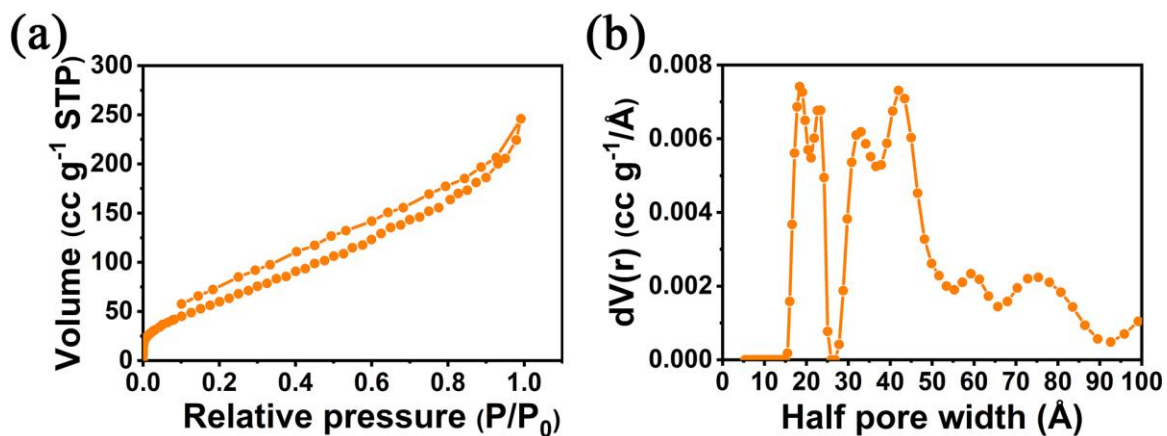


**Figure S3.** (a) N<sub>2</sub> adsorption-desorption isotherms and (b) pore size distribution of MgO<sub>x</sub>-C based on the DFT method.

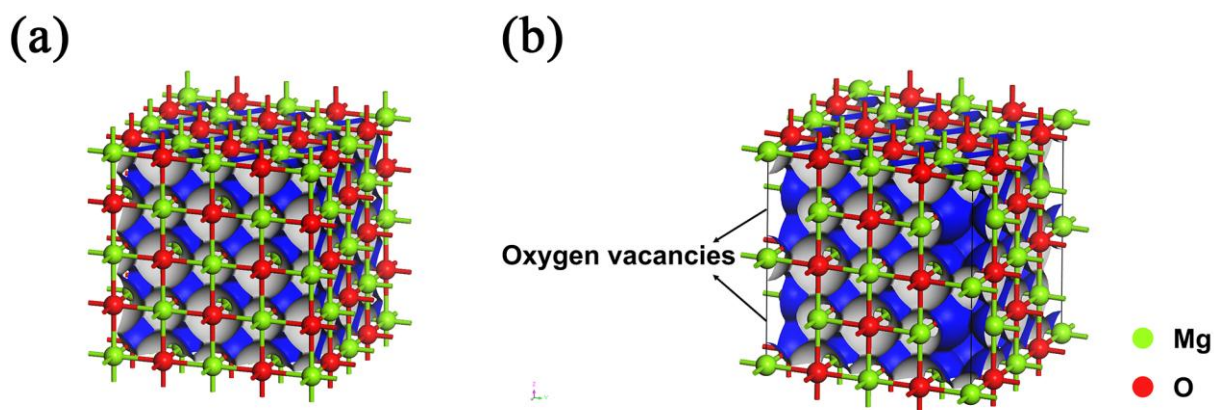


**Figure S4.** Crystal structures of (a) MgO and (b) defective MgO<sub>x</sub>.

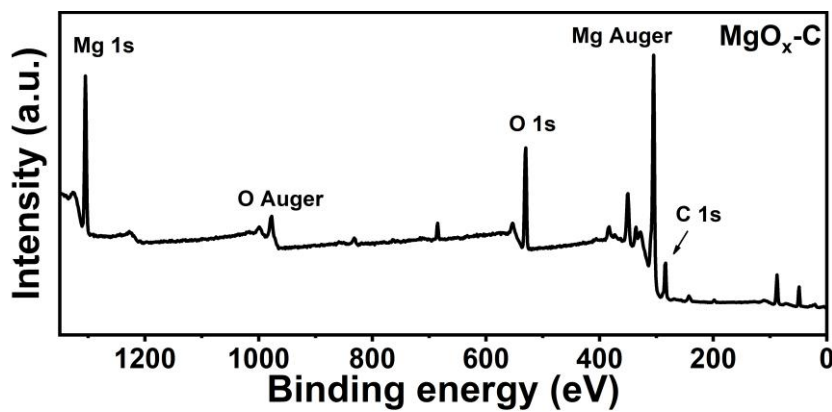


**Figure S5.** Survey XPS spectrum of MgO<sub>x</sub>-C.

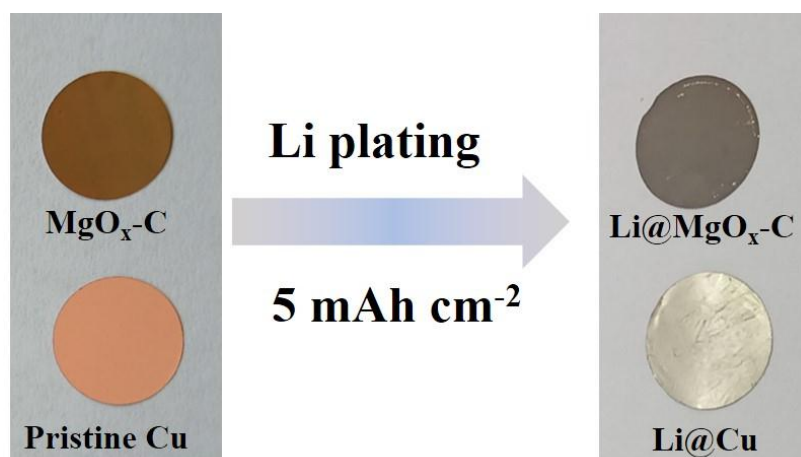


**Figure S6.** Digital photos of Cu current collector with or without  $\text{MgO}_x\text{-C}$  coating before and after Li plating with a capacity of  $5 \text{ mAh cm}^{-2}$ .

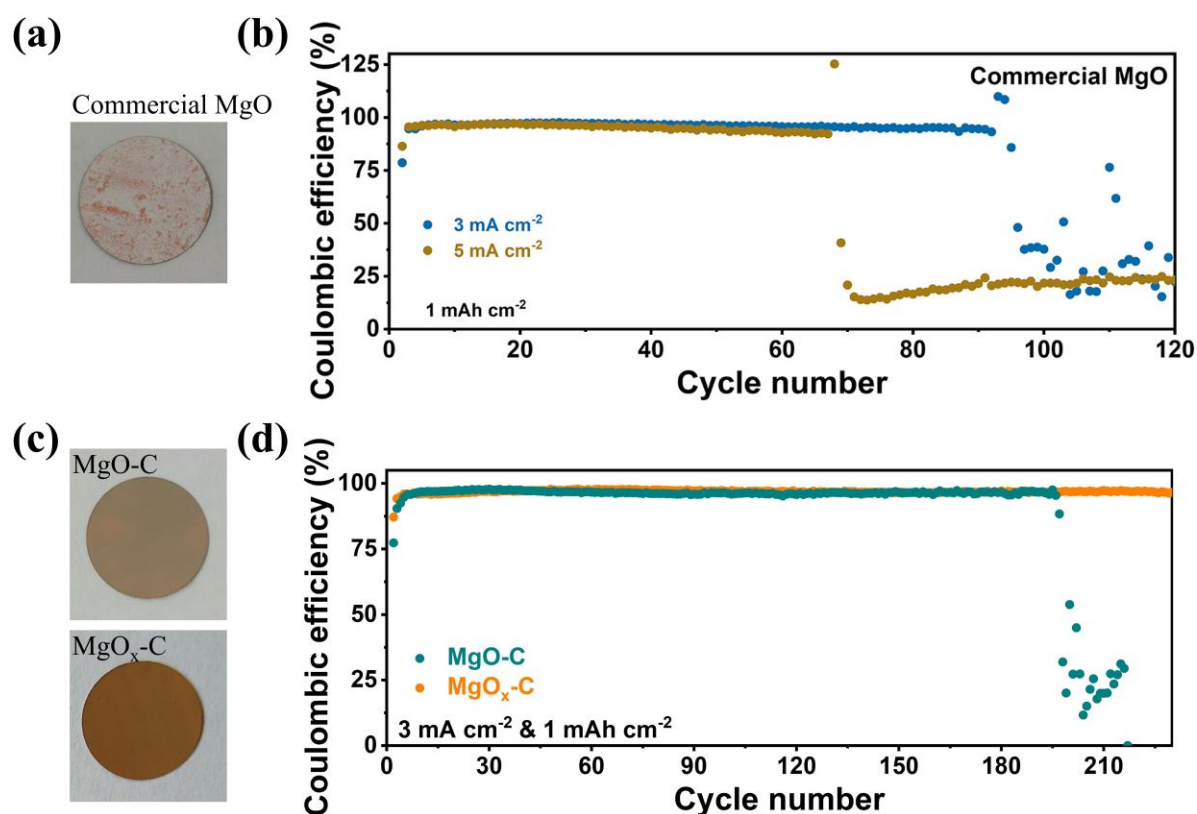


**Figure S7.** (a) Digital photo of Cu current collector with commercial MgO coating. (b) Coulombic efficiency of asymmetric cells with commercial MgO coating at the current densities of 3 and 5 mA cm<sup>-2</sup> with a fixed plating capacity of 1 mAh cm<sup>-2</sup>. (c) Digital images

of MgO-C and MgO<sub>x</sub>-C coatings on Cu foils. (d) Comparison of cycling performance of the electrodes with oxygen defects (MgO<sub>x</sub>-C) and of defect healing (MgO-C) at 3 mA cm<sup>-2</sup> with a capacity of 1 mAh cm<sup>-2</sup>.

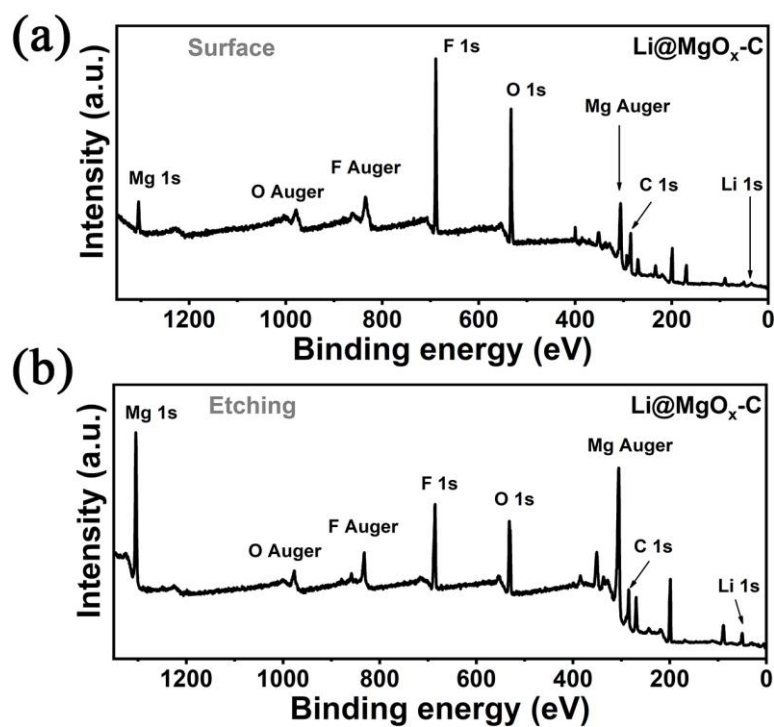


**Figure S8.** Survey XPS spectra of Li@MgO<sub>x</sub>-C (a) without and (b) with surface etching treatment for 10 s.

**Table S1.** Elemental composition (at.%) of Li@MgO<sub>x</sub>-C surface determined by XPS analysis with or without etching treatment.

	Mg (at.%)	O (at.%)	C (at.%)	F (at.%)	Li (at.%)
Surface	4.91	24.47	30.01	18.84	6.75
Etching for 10s	13.72	21.72	23.97	19.29	7.13

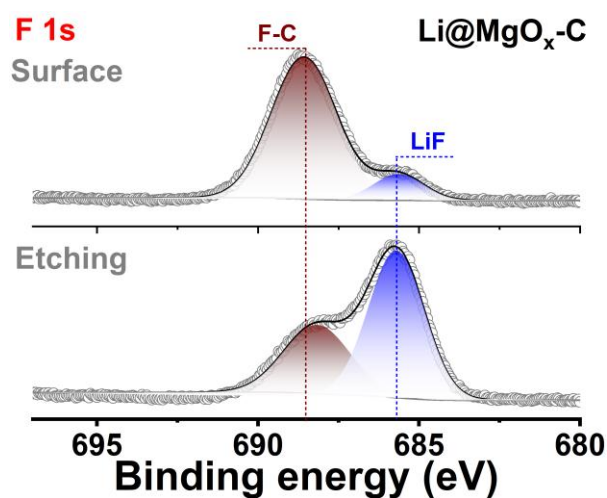


**Figure S9.** High-resolution XPS spectra and deconvolution peaks of F 1s in Li@MgO<sub>x</sub>-C surface with or without surface etching treatment for 10 s.

**Table S2.** Parameters for the calculation of Li<sup>+</sup> transfer number detected by potential impulse and AC impedance techniques

Electrode	$\Delta V$ (mV)	$R_0$ ( $\Omega$ )	$R_s$ ( $\Omega$ )	$I_0$ ( $\mu A$ )	$I_s$ ( $\mu A$ )	$t_{Li^+}$
Li@Cu	4.6	24.58	24.96	109.19	81.77	0.561
Li@MgO <sub>x</sub> -C	4.6	12.04	19.45	95.61	74.43	0.852

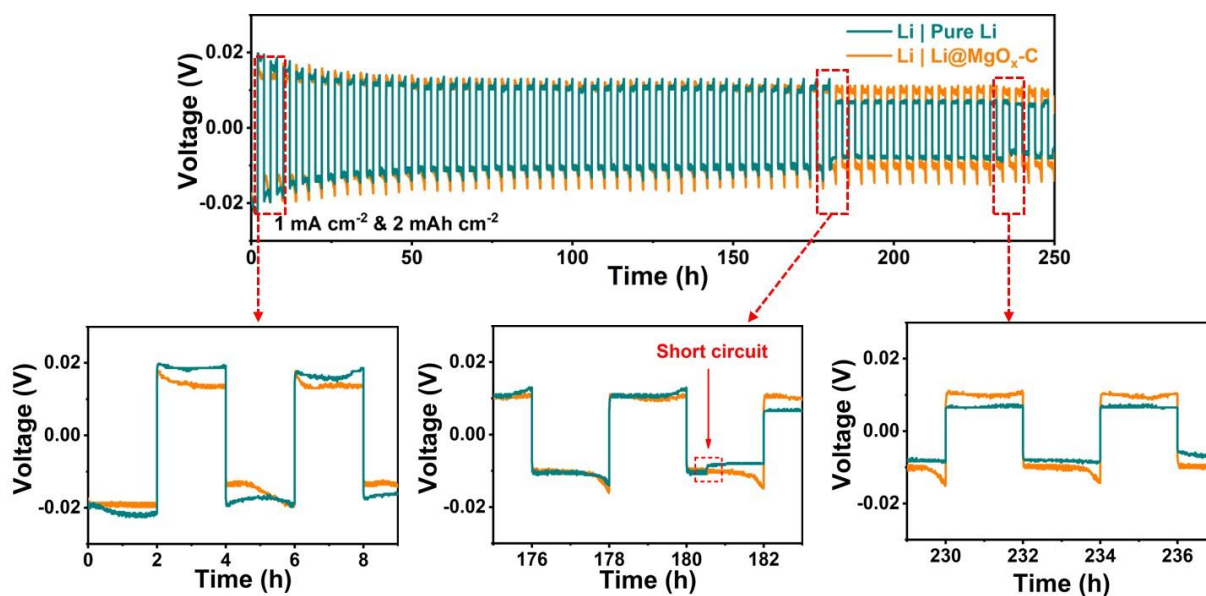


**Figure S10.** Voltage profiles of symmetric cells based on Li@MgO<sub>x</sub>-C and pure Li electrodes at a current density of 1 mA cm<sup>-2</sup> with a fixed capacity of 2 mAh cm<sup>-2</sup>, and (below) corresponding voltage profiles of symmetric cells at different cycling stages.

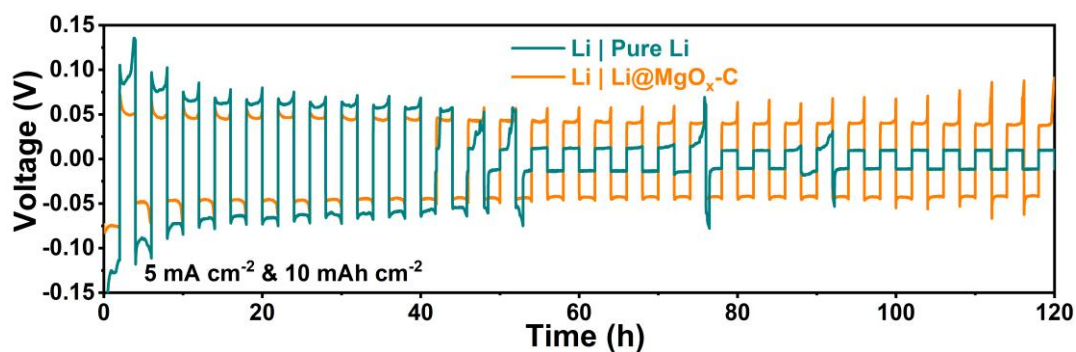


**Figure S11.** Voltage profiles of symmetric cells based on Li@MgO<sub>x</sub>-C and pure Li electrodes at a current density as high as 5 mA cm<sup>-2</sup> with a fixed capacity as high as 10 mAh cm<sup>-2</sup>.

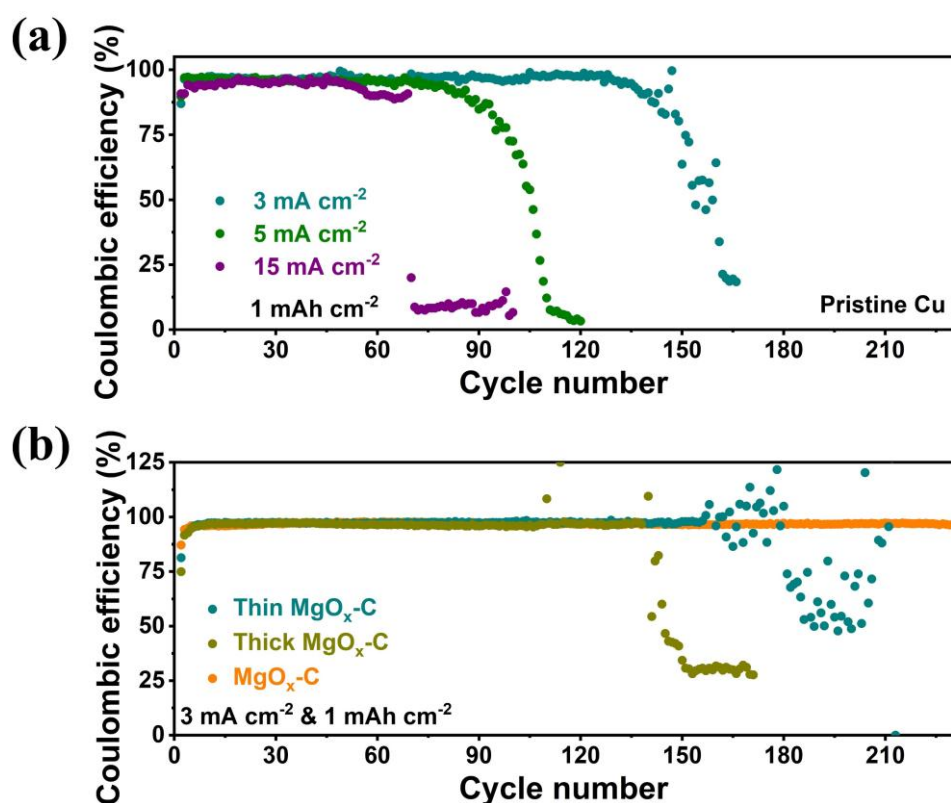


**Figure S12.** (a) Coulombic efficiency plots of asymmetric cells based on pristine Cu electrode at various current densities with a fixed plating capacity of 1 mAh cm<sup>-2</sup>. (b) Comparison of coulombic efficiency plots of asymmetric cells based on MgO<sub>x</sub>-C electrodes with different coating thickness at 3 mA cm<sup>-2</sup> with a fixed plating capacity of 1 mAh cm<sup>-2</sup>.

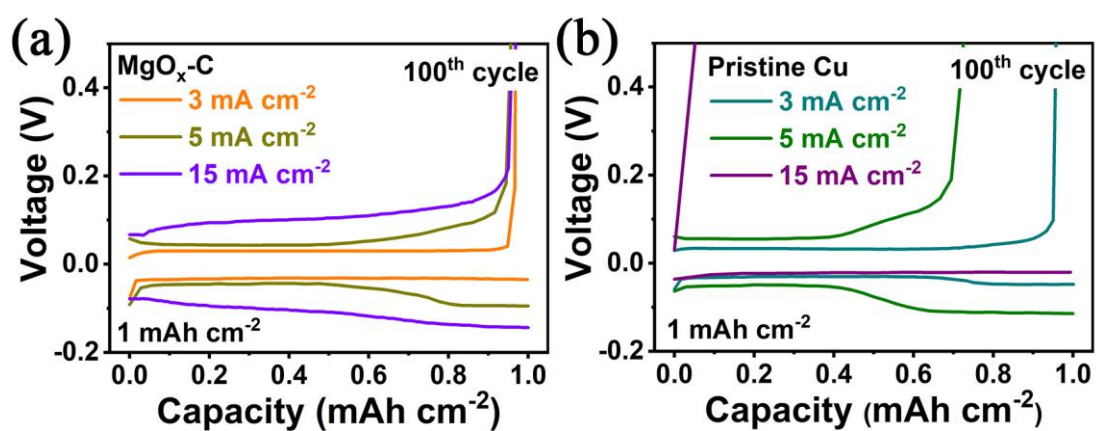


**Figure S13.** Galvanostatic discharge-charge profiles of asymmetric cells based on (a) MgO<sub>x</sub>-C and (b) pristine Cu electrodes at the 100<sup>th</sup> cycle stage under various current densities.

The fluctuation of voltage curves and polarization is associated with the evolution of interface resistance during Li plating/stripping process on  $\text{MgO}_x\text{-C}$ . The higher current density (e.g.  $5 \text{ mA/cm}^2$ ) would cause the rougher electro-deposition especially at the later deposition stage with thicker Li layer, which would remarkably increase the interface resistance and therefore the voltage polarization. The higher current density would also degrade the electric contact during the later electro-stripping process, with the increase of residual holes after Li mass removal. Therefore the increase of voltage polarization is also observed. But over-high current density (e.g.  $15 \text{ mA/cm}^2$ ) would in turn mitigate the roughness of Li deposition due to the local thermal release. Therefore the voltage increase appears to be steady.

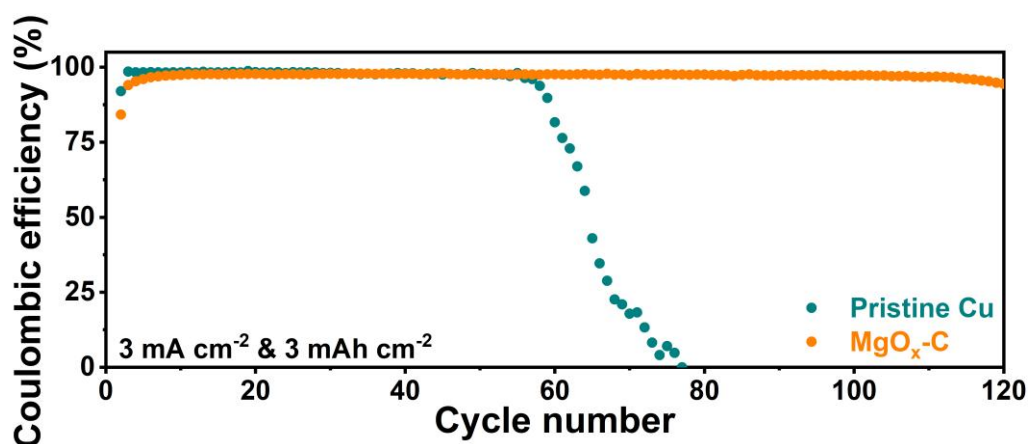


**Figure S14.** Coulombic efficiency plots of Li plating/stripping processes on  $\text{MgO}_x\text{-C}$  and pristine Cu electrodes at  $3 \text{ mA cm}^{-2}$  with a Li plating capacity of  $3 \text{ mAh cm}^{-2}$ .

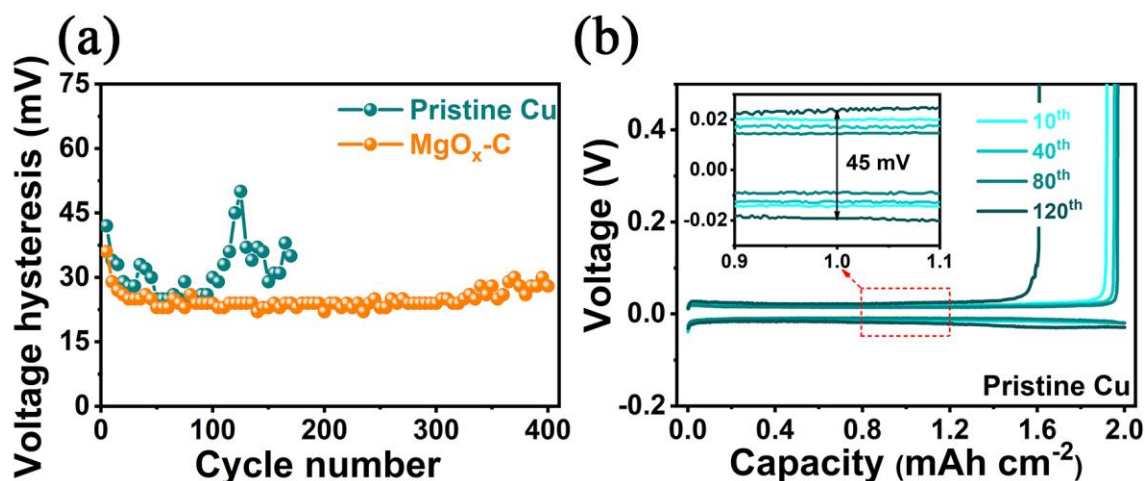


**Figure S15.** (a) Voltage hysteresis evolution of Li plating/stripping on MgO<sub>x</sub>-C and pristine Cu electrodes as a function of cycle number at 1 mA cm<sup>-2</sup> with a plating capacity of 2 mAh cm<sup>-2</sup>. (2) Voltage profiles of Li plating/stripping on pristine Cu electrode at different cycle stages at 1 mA cm<sup>-2</sup> with a plating capacity of 2 mAh cm<sup>-2</sup>.

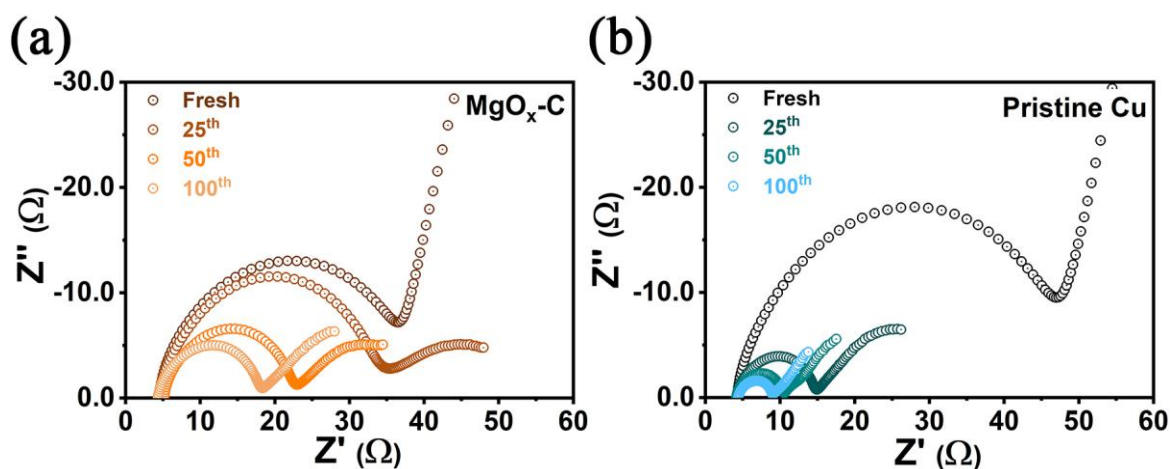


**Figure S16.** Electrochemical impedance spectra of Li/Cu cells based on (a) MgO<sub>x</sub>-C and (b) pristine Cu electrodes after different cycles (at the plating state) at 1 mA cm<sup>-2</sup> with a plating capacity of 2 mAh cm<sup>-2</sup>.

For the tests of interface impedance and voltage hysteresis, the corresponding states of asymmetric Li/Cu cells are different. Specifically, the interface impedance is measured after complete Li plating, and the voltage hysteresis is estimated based on the plateau voltage difference during Li plating and stripping process. In pristine Li/Cu cells, the lithium

dendrites accumulate in the separator with the increase of cycling number especially after complete Li plating, resulting in a micro short circuit and thus a smaller interface impedance. Some lithium dendrites would fall off to form dead lithium in the subsequent stripping process, which would cause the slight increase and fluctuation of voltage hysteresis due to the degradation of electric contact at interface as shown in Figure S15a.

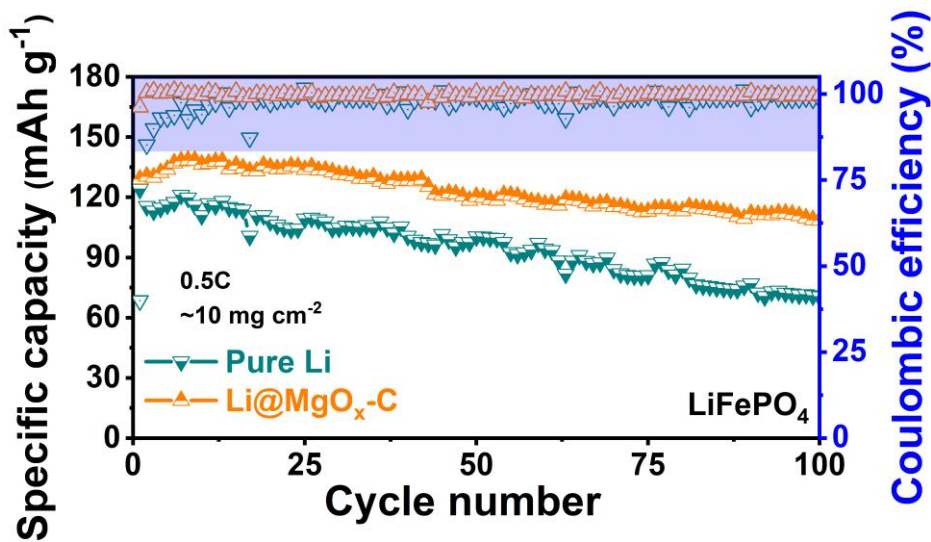


**Figure S17.** Galvanostatic cycling performance of LiFePO<sub>4</sub> full cells based on Li@MgO<sub>x</sub>-C and pure Li anodes at a rate of 0.5 C.

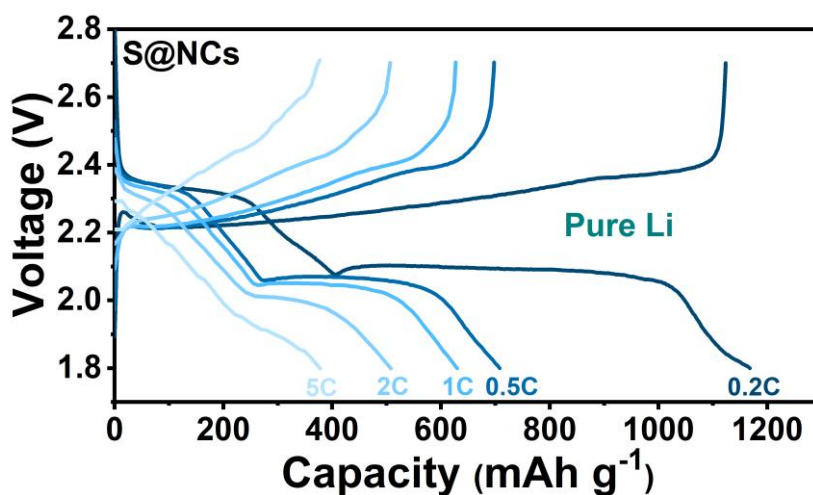


**Figure S18.** Discharge-charge curves of S@NCs full cell based on pure Li anode at various rates.